Earth Surf. Dynam. Discuss., 2, 1023–1046, 2014
www.earth-surf-dynam-discuss.net/2/1023/2014/
doi:10.5194/esurfd-2-1023-2014

Earth Surface Dynamics
Discussions
Open Access

Morphology of the Kosi megafan channels

K. Gaurav[1], F. Métivier[1], O. Devauchelle[1], R. Sinha[2], H. Chauvet[1], M. Houssais[3], and H. Bouquerel[1]

[1]Institute de Physique du Globe de Paris, 1 Rue Jussieu, 75005 Paris CEDEX 05, France
[2]Department of Earth Sciences, Indian Institute of Technology, Kanpur, 208016 UP, India
[3]Department of Earth and Environmental Science, University of Pennsylvania, Philadelphia, PA 19104, USA

Received: 16 September 2014 – Accepted: 19 September 2014 – Published: 1 October 2014

Correspondence to: K. Gaurav (gaurav@ipgp.fr)

Published by Copernicus Publications on behalf of the European Geosciences Union.

Abstract

We study the morphology of streams flowing on the alluvial megafan of the Kosi River in north Bihar, India. All streams develop on a uniform sandy sediment and under a similar climate, allowing for statistically significant comparisons. Our data set includes both channels from the braid of the Kosi River and channels from isolated single-thread rivers. Using an Acoustic Doppler Current Profiler, we measure the width, depth and water discharge of the channels. Their average slope is also acquired with a kinematic GPS. These morphological characteristics are strongly correlated with the discharge. However, rescaling the data according to the threshold channel theory removes most of this dependency. The rescaled data suggest that the threads of the Kosi River braid are morphologically similar to isolated channels.

1 Introduction

Alluvial rivers form single or multiple-threads channels (e.g. Leopold et al., 1957; Van den Berg, 1995; Métivier and Barrier, 2012). In nature, the same river can develop both patterns along its course, and both can coexist on the same alluvial surface (Garde and Raju, 2000; Singh et al., 1993). The process by which the river selects a specific pattern remains a matter of debate. Possible governing parameters are water flow, sediment type and riparian vegetation (Parker, 1978; Gran and Paola, 2001; Tal and Paola, 2007; Métivier and Barrier, 2012). Typically, an alluvial river with a low sediment discharge tends to form a single-thread channel, whereas a higher sediment discharge often generates a multiple-threads channel, referred to as a braided river (Mackin, 1948; Church, 1975; Germanoski and Schumm, 1993; Schumm, 1985; Eaton et al., 2010; Seizilles et al., 2013).

Previous studies have shown that individual threads in braided rivers are morphologically comparable, within the same channel (Fahnestock, 1963; Church, 1975; Ashmore, 1982; Mosley, 1983; Bridge and Gabel, 1992; Ferguson, 1993; Bridge, 1993). Laboratory experiments accord with this observation (Reitz et al., 2014). This suggests that a braided river is collection of distinct, but similar, threads. Therefore, it might be instructive to compare the individual threads of a braided river with single-thread channels, as the latter could provide a useful analogue of the former. Indeed, the mechanisms by which an isolated channel selects its morphology have been extensively studied (Glover and Florey, 1951; Henderson, 1963; Parker, 1978; Parker et al., 2007; Seizilles et al., 2013). Can we apply this knowledge to the individual threads of braided rivers? To answer this question, we need to compare single-thread channels with braided threads, all other things being equal.

Here we compare the morphology of single-thread channels with braided threads of the Kosi River in north Bihar, India. All channels spread over the same megafan composed of homogeneous sandy deposits, and are submitted to the same climate. We report the measurements of width, depth, slope and water discharge from 19 single-thread channels and 35 braided threads. Finally, we use the threshold channels theory to rescale our data and evaluate, for both channel patterns, the statistical distributions of their morphological characteristics.

The large dimension of the Kosi River, its braided and single-thread morphology, its sandy bed, makes it an ideal field site to conduct this study.

2 The Kosi River megafan

The megafan of the Kosi River spans over 10 351 km^2 of the northern Bihar plain, India (Fig. 1). It results from the deposition of Himalayan sediments by the Kosi River. These sediments are essentially composed of quartz grains with a median size of 270 µm in the proximal part of the fan, and 98 µm in its distal part. A series of avulsions has build an almost conical fan surface, which longitudinal slope varies from about 8×10^{-4} at the apex, to 6×10^{-5} near the toe (Gole and Chitale, 1966; Wells and Dorr, 1987; Chakraborty et al., 2010; Singh et al., 1993).

Today, the main flow of the Kosi River is located at the western flank of the fan, where it is confined by an artificial embankment. Within this embankment, the Kosi River is braided along most of its course, and turns into a meandering single-thread channel near its confluence with the Ganga River (Seni, 1980; Gohain, 1990; Singh et al., 1993; DeCelles and Cavazza, 1999; Chakraborty et al., 2010).

In addition to the Kosi River itself, tens of isolated single-thread rivers spread across the entire fan surface. These channels appear in the remnants of the Kosi River past courses. Most of them are fed either by groundwater, or by seepage from the Kosi River (Sinha et al., 2013; Chakraborty et al., 2010). Hereafter, we refer to them as seepage channels.

Seepage channels and threads of the Kosi River flow over the sediment composing the fan, and therefore their beds exhibit a similar composition and granulometry.

3 Field measurements

During the monsoon of 2012, and just after the monsoon of 2013, we have collected the width, depth and discharge of 54 threads of the Kosi River megafan. The monsoon discharge is likely to be the formative discharge under the climate of northern Bihar (Fig. 2).

We use an Acoustic Doppler Current Profiler to measure the hydraulic geometry and the discharge of the channels (RD-instruments RioGrande 1.2 MHz). This instrument features four transducers with a fixed beam angle of 20° with respect to the vertical (Morlock, 1996; Parsons et al., 2005; Simpson, 2001). The ADCP emits acoustic pulses through the water column, and records the pusles reflected by scatterers, such as bubbles or sediment particles. Its beams are divided into equal-size bins of 5 to 25 cm. Based on the Doppler frequency shift, it then computes the flow velocity (Rennie and Villard, 2004; Parsons et al., 2005; Chauvet et al., 2011). In addition, we complemented the ADCP with an external echo-sounder to record the water depth (Tritech) (Richardson and Thorne, 2001).

For this study, we have measured 54 transects; 35 were from braided threads, and 19 where from isolated threads (Tables A1 and A2). To do so, we deploy the ADCP on an inflatable motor boat and cross the channel perpendicularly to the flow direction, while a hand-held GPS records the boat's position.

To assess the measurement uncertainty, we have crossed 20 channels twice, thus acquiring two independent transects for each channel. Based on these redundant measurements, we find a relative error of about 10, 15, 5, and 12 % for the width, depth, mean velocity and discharge respectively.

We could not access the smaller channels by boat, and we measured their characteristics manually. To do so, we first measure the water depth every 0.5 m across the channel with a wading rod. This method yields a precision of about 2 cm. We then measure the surface velocity of the flow by dropping a float and measuring its travel time over a fixed distance (10 to 20 m), and repeat this procedure three times at the same location. To take the logarithmic velocity profile into account, we multiply the surface velocity by 0.6 to approximate the depth-averaged velocity (Sanders, 1998). The uncertainty on this value is about 11 %.

Finally, we have measured the grain-size distribution and the slope of 4 braided threads and 2 isolated threads (Table A3). We have sieved the sediment sample to distribute the grains between 6 size categories, from 0.063 to 0.315 mm. To measure the slope of a channel, we embark a real-time kinematic GPS on the boat (Trimble-R8), and travel downstream over at least 7 km. Our measurement therefore yields the slope of the water surface.

4 Results and discussion

4.1 Cross sections

Regardless of their size, single-thread channels from the Kosi River fan are shallow, with an aspect ratio ranging from 10 to 100 (Fig. 3). At first glance, the cross sections

of seepage channels appear similar in shape to that of the single-thread reach of the Kosi River. The flow velocity is of the order of 1 m s^{-1}, with a maximum near the center of the channel.

The cross-section of braided threads is typically more intricate (Fig. 4). Most braided threads exhibit significant variations of the bed topography, which sometimes reduce the depth to less than 10 % of the maximum depth. If we consider that the shallow areas correspond to bars separating the channel into multiple threads, the cross section of each of the resulting threads resemble that of single-thread channels.

By definition, a braided river is a collection of intertwined threads. Decomposing the channel into individual threads, however, is a somewhat arbitrary procedure, if only because the wetted area depends on the discharge (Mosley, 1983; Ashmore, 2013). One could equate threads with water bodies, in which case each cross section on Fig. 4 would correspond to an individual thread. This definition is specially convenient when using aerial images of the channel. Here, the detailed topography of the cross-section permits a finer decomposition of the channel.

Our objective is to compare the morphology of isolated single threads to that of braided threads. Accordingly, we need to decompose the braided channel into elements comparable to single threads. To do so, we manually detect bars separating channels based on their elevation relative to the deeper part of the bed. Wherever the water depth is less than 10 % of the maximum channel depth, we consider this area to be a bar, and split the channel accordingly (Fig. 4).

4.2 Regime relations for the Kosi fan threads

Once we have decomposed all cross sections into individual threads, we can measure their morphological characteristics. We approximate the width W of a thread by the extension of the transect we were able to acquire. At most, the bank was located 10 m away from the end of the transect. Similarly, we calculate the average depth H and the water discharge Q of a thread by integrating over the corresponding transect.

Not surprisingly, the size of a thread increases with discharge (Fig. 5). Conversely, its slope S decreases with discharge. We observe no obvious difference between single and braided threads, and all data points seem to gather around single curves, despite considerable scatter. This observation suggests that single and braided threads might share common regime relations (Lacey, 1930; Parker et al., 2007).

One of the simplest set of regime relations for single-thread alluvial channels derives from the threshold hypothesis (Glover and Florey, 1951; Henderson, 1963; Seizilles et al., 2013). This theory assumes that the channel sediment is exactly at the threshold of motion. In other words, the combination of gravity and flow-induced shear stress hardly suffices to displace a sediment grain. For a specific discharge, this equilibrium sets the width, the depth and the longitudinal slope of the channel. The corresponding regime relations are (Seizilles, 2013):

$$W = \frac{\pi d_s}{\mu} \left(\frac{\theta_t (\rho_s - \rho)}{\rho} \right)^{1/4} \sqrt{\frac{3 C_f}{2^{3/2} \mathcal{K}\left[1/2\right]}} Q_*^{1/2} \qquad (1)$$

$$H = \frac{d_s}{\pi} \left(\frac{\theta_t (\rho_s - \rho)}{\rho} \right)^{1/4} \sqrt{\frac{3\sqrt{2} C_f}{\mathcal{K}\left[1/2\right]}} Q_*^{1/2} \qquad (2)$$

$$S = \mu^{3/4} \sqrt{\frac{\mathcal{K}\left[1/2\right] 2^{3/2}}{3 C_f}} Q_*^{-1/2} \qquad (3)$$

where $Q_* = Q/\sqrt{g d_s^5}$ is the dimensionless water discharge (Parker, 1979; Parker et al., 2007; Wilkerson and Parker, 2010). Here, we have chosen the simplest possible formulation of the threshold theory (Métivier and Barrier, 2012). In particular, we assume that the Chézy friction factor $1/C_f \approx 10$ is independent of the flow depth. All other parameters are approximately constant for the channels of the Kosi River fan: $\theta_t \approx 0.3$ is the threshold Shields parameter, $g \approx 9.8\,\mathrm{m\,s^{-2}}$ is the acceleration of gravity, $\mu \approx 0.7$ is Coulomb's coefficient of friction, $d_s \approx 0.19\,\mathrm{mm}$ is the sediment grain size,

$\rho \approx 1000\,\mathrm{kg\,m^{-3}}$ is the density of water and $\rho_s \approx 2650\,\mathrm{kg\,m^{-3}}$ is the density of quartz. Finally, $\mathcal{K}(1/2) \approx 1.85$ is the elliptic integral of the first kind.

We can now compare the threshold theory with our data set (green line on Fig. 5). Most threads are wider than predicted, by a factor of about 2. They are also significantly shallower (factor of about 4) and about 15 times steeper. This discrepancy is not surprising since the threshold hypothesis corresponds to a vanishing sediment discharge, whereas the entire Kosi River transports about 43 Mt of sediments every year (Sinha, 2009).

However, the threshold theory predicts reasonably the trend of the threads morphology as the discharge increases. To evaluate the quality of this prediction, we now fit the prefactors of the threshold relations (1), (2) and (3) to the data, while keeping their theoretical exponent (grey line on Fig. 5). The resulting semi-empirical relations accord with observations, considering the large dispersion of the data.

4.3 Detrending

The semi-empirical regime relations based on the threshold theory represent analytically the dependency of a thread's morphological parameters with respect to discharge. Therefore, we can use them to detrend our data with respect to discharge. To do so, we define the dimensionless width W_*, depth H_* and slope S_* as

$$W_* = \frac{W}{d_s \sqrt{Q_*}} = \frac{W (g d_s)^{1/4}}{\sqrt{Q}} \qquad (4)$$

$$H_* = \frac{H}{d_s \sqrt{Q_*}} = \frac{H (g d_s)^{1/4}}{\sqrt{Q}} \qquad (5)$$

$$S_* = S \sqrt{Q_*} = \frac{S \sqrt{Q}}{g^{1/4} d_s^{5/4}}. \qquad (6)$$

As expected, none of the dimensionless parameters above depends significantly on the water discharge (Fig. 6). To evaluate the residual trend and its statistical significance, we artificially produce smaller data sets by bootstrapping, and fit a power law on them. The mean residual exponent is -0.042 ± 0.06 for the dimensionless width, and -0.17 ± 0.04 for the depth (standard deviation). The slope data are too scarce to use bootstrapping, but they do not suggest that there is any residual exponent. Thus, based on our data set, only the dimensionless depth shows a residual correlation with discharge, and it is very weak.

4.4 Braided threads vs. Single threads

Presuming the dimensionless parameters W_*, H_* and S_* are all independent from the water discharge, we may treat our data set as a sample from a statistically uniform ensemble. Accordingly, we can calculate the distribution of each parameter for braided threads and for single threads independently (histograms on Fig. 6). Due to the large scatter in our data, these distribution are better expressed in terms of the common logarithm of the parameters.

The distributions of the dimensionless width W_* of the braided threads resemble that of the single threads, considering the size of our data set. Their mean value and standard deviation are $\langle \log_{10} W_* \rangle \approx 0.31$ and $\sigma(\log_{10} W_*) \approx 0.2$ for braided threads, and $\langle \log_{10} W_* \rangle \approx 0.27$ and $\sigma(\log_{10} W_*) \approx 0.2$ for single threads. The two distributions are thus statistically equivalent. Similarly, despite the slight residual trend of the data (Sect. 4.3), the distributions of dimensionless depth are also equivalent: $\langle \log_{10} H_* \rangle \approx -1.6$ and $\sigma(\log_{10} H_*) \approx 0.2$ for braided threads, and $\langle \log_{10} H_* \rangle \approx -1.4$ and $\sigma(\log_{10} H_*) \approx 0.2$ for single threads.

The dimensionless slope of braided threads is about three times higher than that of single threads. However, our data set contains only four values for braided threads, and two values for single threads. Therefore, we cannot draw any statistically significant conclusion regarding the slope distributions.

5 Conclusions

The simple scaling laws based on the threshold channel theory suffice to account for most of the influence of water discharge on the size of the alluvial threads of the Kosi River fan. After rescaling their morphological characteristics accordingly, we find no significant difference between single threads and threads from a braided channel. This finding extends the previously observed similarity between threads in a braided channel to isolated channels in a comparable environment. If confirmed, this observation would indicate that the basic mechanisms controlling the thread morphology are the same in both channel types.

Such mechanisms are still to be elucidated though. Indeed, the measurements from the Kosi River fan exhibit a large and unexplained dispersion, which is clearly visualized by plotting the threads's aspect ratio as a function of discharge (Fig. 7). Since width and depth scale similarly, their ratio is naturally detrended (Sect. 4.3). Braided threads tend to have a higher aspect ratio than single threads, in accordance with previous studies (Schumm, 1968; Eaton et al., 2010; Métivier and Barrier, 2012). However, this slight difference is overwhelmed by considerable scatter (from about 10 to 300). This dispersion is not correlated with water discharge, indicating that another parameter, at least, influences the morphology of the threads.

In addition to water discharge, the sediment load is known to influence the aspect ratio of alluvial channels (Smith and Smith, 1984; Mueller and Pitlick, 2005; Métivier and Barrier, 2012). We may thus reasonably guess that variations in the sediment load are responsible for the dispersion of the threads's aspect ratio. The Kosi River fan would be an ideal field site to test this hypothesis, provided we can measure accurately the sediment discharge of its channels. Such field measurements are the subject of present work.

Acknowledgements. This work was funded by the Indo-French Centre for Promotion of Advanced Research (CEFIPRA) through grant 4500-W1. We also thank the engineers and the staff of the Kosi River Project for their support in the field.

References

Ashmore, P. E.: Laboratory modelling of gravel braided stream morphology, Earth Surf. Proc. Land., 7, 201–225, 1982. 1024

Ashmore, P. E.: Treatise on Geomorphology, vol. 9 of Fluvial Geomorphology, Academic Press, San Diego, CA, 289–312, 2013. 1028

Bridge, J. S.: The interaction between channel geometry, water flow, sediment transport and deposition in braided rivers, Geol. Soc. Sp., 75, 13–71, 1993. 1024

Bridge, J. S. and Gabel, S. L.: Flow and sediment dynamics in a low sinuosity, braided river: Calamus River, Nebraska Sandhills, Sedimentology, 39, 125–142, 1992. 1024

Chakraborty, T., Kar, R., Ghosh, P., and Basu, S.: Kosi megafan: historical records, geomorphology and the recent avulsion of the Kosi River, Quatern. Int., 227, 143–160, 2010. 1025, 1026

Chauvet, H., Metivier, F., and Limare, A.: Cavitation bubbles: a tracer for turbulent mixing in large rivers, River, Coastal and Estuarine Morphodynamics, RCEM2011, Tsinghua University Press, Beijing, 2011. 1026

Church, M.: Proglacial fluvial and lacustrine environments, Special Publications of SEPM, Glaciofluvial and Glaciolacustrine Sedimentation (SP23), 1975. 1024

DeCelles, P. and Cavazza, W.: A comparison of fluvial megafans in the Cordilleran (Upper Cretaceous) and modern Himalayan foreland basin systems, Geol. Soc. Am. Bull., 111, 1315–1334, 1999. 1026

Eaton, B., Millar, R. G., and Davidson, S.: Channel patterns: braided, anabranching, and single-thread, Geomorphology, 120, 353–364, 2010. 1024, 1032

Fahnestock, R. K.: Morphology and hydrology of a glacial stream – White River, Mount Rainier, US Government Printing Office, Washington, 1963. 1024

Ferguson, R.: Understanding braiding processes in gravel-bed rivers: progress and unsolved problems, Geol. Soc. Sp., 75, 73–87, 1993. 1024

Garde, R. J. and Raju, K. R.: Mechanics of sediment transportation and alluvial stream problems, Taylor and Francis, New Delhi, 2000. 1024

Germanoski, D. and Schumm, S.: Changes in braided river morphology resulting from aggradation and degradation, J. Geol., 101, 451–466, 1993. 1024

Glover, R. E. and Florey, Q.: Stable channel profiles, Hydraulic laboratory report HYD no. 325, US Department of the Interior, Bureau of Reclamation, Design and Construction Division, 1951. 1025, 1029

Gohain, K.: Morphology of the Kosi megafan, in: Alluvial Fans – A Field Approach, edited by: Rachocki, A. H. and Church, M., John Wiley and Sons, Chichester, 151–178, 1990. 1026

Gole, C. V. and Chitale, S. V.: Inland delta building activity of Kosi river, J. Hydr. Eng. Div.-ASCE, 92, 111–126, 1966. 1025

Gran, K. and Paola, C.: Riparian vegetation controls on braided stream dynamics, Water Resour. Res., 37, 3275–3283, 2001. 1024

Henderson, F. M.: Stability of alluvial channels, T. Am. Soc. Civ. Eng., 128, 657–686, 1963. 1025, 1029

Lacey, G.: Stable channels in alluvium (Includes Appendices), in: Minutes of the Proceedings, vol. 229, Thomas Telford, Proceedings of the Institution of Civil Engineers, Landoon, 259–292, 1930. 1029

Leopold, L. B., Wolman, M. G., Wolman, M. G., and Wolman, M. G.: River channel patterns: braided, meandering, and straight, US Government Printing Office, Washington, D.C., 1957. 1024

Mackin, J. H.: Concept of the graded river, Geol. Soc. Am. Bull., 59, 463–512, 1948. 1024

Métivier, F. and Barrier, L.: Alluvial Landscape Evolution: What Do We Know About Metamorphosis of Gravel-Bed Meandering and Braided Streams?, Gravel-Bed Rivers: Processes, Tools, Environments, John Wiley & Sons, Ltd, Chichester, UK, 474–501, 2012. 1024, 1029, 1032

Morlock, S. E.: Evaluation of acoustic Doppler current profiler measurements of river discharge, Water-Resources Investigations Report 95-4218, US Department of the Interior, US Geological Survey, Indianapolis, Indiana, 1996. 1026

Mosley, M.: Response of braided rivers to changing discharge, J. Hydrol., 22, 18–67, 1983. 1024, 1028

Mueller, E. R. and Pitlick, J.: Morphologically based model of bed load transport capacity in a headwater stream, J. Geophys. Res.-Earth, 110, F02016, doi:10.1029/2003JF000117, 2005. 1032

Parker, G.: Self-formed straight rivers with equilibrium banks and mobile bed, Part 1, The sand-silt river, J. Fluid Mech., 89, 109–125, 1978. 1024, 1025

Parker, G.: Hydraulic geometry of active gravel rivers, J. Hydr. Eng. Div.-ASCE, 105, 1185–1201, 1979. 1029

Parker, G., Wilcock, P. R., Paola, C., Dietrich, W. E., and Pitlick, J.: Physical basis for quasi-universal relations describing bankfull hydraulic geometry of single-thread gravel bed rivers, J. Geophys. Res.-Earth, 112, F04005, doi:10.1029/2006JF000549, 2007. 1025, 1029

Parsons, D., Best, J., Orfeo, O., Hardy, R., Kostaschuk, R., and Lane, S.: Morphology and flow fields of three-dimensional dunes, Rio Paraná, Argentina: results from simultaneous multibeam echo sounding and acoustic Doppler current profiling, J. Geophys. Res.-Earth, 110, F04S03, doi:10.1029/2004JF000231, 2005. 1026

Reitz, M., Jerolmack, D., Lajeunesse, E., Limare, A., Devauchelle, O., and Métivier, F.: Diffusive evolution of experimental braided rivers, Phys. Rev. E, 89, 052809, doi:10.1103/PhysRevE.89.052809 2014. 1025

Rennie, C. D. and Villard, P. V.: Site specificity of bed load measurement using an acoustic Doppler current profiler, J. Geophys. Res.-Earth, 109, F03003, doi:10.1029/2003JF000106, 2004. 1026

Richardson, W. R. and Thorne, C. R.: Multiple thread flow and channel bifurcation in a braided river: Brahmaputra–Jamuna River, Bangladesh, Geomorphology, 38, 185–196, 2001. 1026

Sanders, L. L.: Manual of field hydrogeology, UpperSaddle River, Prentice-Hall Inc., New Jersey, 1998. 1027

Schumm, S.: River adjustment to altered hydrologic regimen, Murrumbidgee River and paleochannels, Prof. Pap. 898, USGS, Australia, 1968. 1032

Schumm, S.: Patterns of alluvial rivers, Annu. Rev. Earth Pl. Sc., 13, 5–27, 1985. 1024

Seizilles, G.: Forme d'équilibre d'une rivière, Ph.D. thesis, Paris, 2013. 1029

Seizilles, G., Devauchelle, O., Lajeunesse, E., and Métivier, F.: Width of laminar laboratory rivers, Phys. Rev. E, 87, 052204, doi:10.1103/PhysRevE.87.052204, 2013. 1024, 1025, 1029

Seni, S. J.: Sand-body geometry and depositional systems, Ogallala Formation, Texas, 1980. 1026

Simpson, M. R.: Discharge measurements using a broad-band acoustic Doppler current profiler, US Department of the Interior, Open-File Report 01-1, US Geological Survey, USGS, Sacramento, California, 2001. 1026

Singh, H., Parkash, B., and Gohain, K.: Facies analysis of the Kosi megafan deposits, Sediment. Geol., 85, 87–113, 1993. 1024, 1025, 1026

Sinha, R.: The great avulsion of Kosi on 18 August 2008, Curr. Sci. India, 97, 429–433, 2009. 1030

Sinha, R., Gaurav, K., Chandra, S., and Tandon, S.: Exploring the channel connectivity structure of the August 2008 avulsion belt of the Kosi River, India: application to flood risk assessment, Geology, 41, 1099–1102, 2013. 1026

Smith, N. D. and Smith, D. G.: William River: an outstanding example of channel widening and braiding caused by bed-load addition, Geology, 12, 78–82, 1984. 1032

Tal, M. and Paola, C.: Dynamic single-thread channels maintained by the interaction of flow and vegetation, Geology, 35, 347–350, 2007. 1024

Van den Berg, J. H.: Prediction of alluvial channel pattern of perennial rivers, Geomorphology, 12, 259–279, 1995. 1024

Wells, N. A. and Dorr, J. A.: Shifting of the Kosi river, northern India, Geology, 15, 204–207, 1987. 1025

Wilkerson, G. V. and Parker, G.: Physical basis for quasi-universal relationships describing bankfull hydraulic geometry of sand-bed rivers, J. Hydraul. Eng.-ASCE, 137, 739–753, 2010. 1029

Discussion Paper | Discussion Paper | Discussion Paper | Discussion Paper |

Table A1. Measurements of width, depth, velocity and water discharge on braided threads of the Kosi fan.

Year	River	Instrument	Width (m)	Depth (m)	Velocity ($m\,s^{-2}$)	Discharge ($m^3\,s^{-1}$)	Latitude (dd)	Longitude (dd)
2012	Main Kosi	ADCP	351	1.8	1.6	1114	26.702	87.074
2012	Main Kosi	ADCP	139	1.8	0.8	208	26.649	87.050
2012	Main Kosi	ADCP	147	2.9	0.7	277	26.649	87.049
2012	Main Kosi	ADCP	29	1.7	0.8	45	26.048	86.485
2012	Main Kosi	ADCP	404	2.3	1.5	1338	26.048	86.484
2012	Main Kosi	ADCP	391	2.2	1.4	1250	26.048	86.463
2013	Main Kosi	ADCP	1148	5.2	0.5	4088	26.525	86.927
2013	Main Kosi	ADCP	77	0.4	0.5	12	26.491	86.916
2013	Main Kosi	ADCP	196	2.3	1.3	594	26.492	86.918
2013	Main Kosi	ADCP	198	2.4	1.4	602	26.492	86.918
2013	Main Kosi	ADCP	90	0.4	0.5	18	26.491	86.916
2013	Main Kosi	ADCP	46	0.4	0.9	18	26.49	86.936
2013	Main Kosi	ADCP	97	1.5	1.1	168	26.423	86.840
2013	Main Kosi	ADCP	151	2.6	1.6	640	26.421	86.846
2013	Main Kosi	ADCP	186	2.9	0.5	252	26.422	86.853
2013	Main Kosi	ADCP	29	0.7	1	29	26.357	86.732
2013	Main Kosi	ADCP	156	1.8	1.1	277	26.356	86.733
2013	Main Kosi	ADCP	100	0.5	0.9	33	26.355	86.734
2013	Main Kosi	ADCP	118	1.4	1.3	189	26.312	86.672
2013	Main Kosi	ADCP	62	1.3	0.3	26	26.347	86.707
2013	Main Kosi	ADCP	86	1.1	1.2	95	26.346	86.707
2013	Main Kosi	ADCP	58	2.6	1.1	175	26.377	86.789
2013	Main Kosi	ADCP	67	2.8	1.2	190	26.376	86.788
2013	Main Kosi	ADCP	554	1.7	1	752	26.375	86.792
2013	Main Kosi	ADCP	79	0.5	0.5	16	26.366	86.776
2013	Main Kosi	ADCP	96	1.5	0.9	101	26.338	86.763
2013	Main Kosi	ADCP	430	2.1	0.8	736	25.834	86.443
2013	Main Kosi	ADCP	98	1.2	1.1	133	25.817	86.416
2013	Main Kosi	ADCP	91	0.8	0.8	45	25.812	86.447
2013	Main Kosi	ADCP	28	0.9	0.6	15	25.81	86.443
2013	Main Kosi	ADCP	41	0.7	0.7	19	25.808	86.441
2013	Main Kosi	ADCP	134	1.3	0.9	174	25.807	86.437
2013	Main Kosi	ADCP	63	0.8	0.6	29	25.807	86.438
2013	Main Kosi	ADCP	38	2.2	1.1	87	26.047	86.485
2013	Main Kosi	ADCP	381	2.3	1.3	960	26.064	86.482

Table A2. Measurements of width, depth, velocity and water discharge on single-thread channels of the Kosi fan.

Year	River	Instrument	Width (m)	Depth (m)	Velocity ($m\,s^{-2}$)	Discharge ($m^3\,s^{-1}$)	Latitude (dd)	Longitude (dd)
2013	Main Kosi	ADCP	345	4.6	1.3	2462	25.517	86.737
2013	Main Kosi	ADCP	558	3.9	1.1	2819	25.507	86.737
2013	Main Kosi	ADCP	121	4.4	0.8	409	25.518	86.733
2013	Main Kosi	ADCP	519	3.3	0.9	2252	25.419	87.169
2013	Main Kosi	ADCP	370	2.3	1	713	25.683	86.542
2013	Seepage Channel	ADCP	60	2.3	0.8	111	25.877	86.951
2013	Seepage Channel	ADCP	68	1.8	0.7	113	25.857	86.941
2013	Seepage Channel	ADCP	65	2	0.7	114	25.857	86.941
2013	Seepage Channel	ADCP	68	2.3	0.6	113	25.851	86.934
2013	Seepage Channel	ADCP	30	0.7	0.8	20	25.953	86.959
2013	Seepage Channel	ADCP	52	3.7	0.6	123	25.786	86.887
2013	Seepage Channel	ADCP	31	3	0.7	78	25.777	86.870
2013	Seepage Channel	Float	30	0.7	0.4	9	26.519	87.029
2013	Seepage Channel	Float	72	0.4	0.6	16	26.534	87.028
2013	Seepage Channel	Float	50	0.5	0.4	9	26.505	87.028
2013	Seepage Channel	Float	32	0.8	0.3	8	26.519	87.029
2013	Seepage Channel	Float	51	1.3	0.2	11	26.444	86.998
2013	Seepage Channel	Float	40	1.5	0.3	18	26.443	86.995
2013	Seepage Channel	Float	73	0.7	0.2	9	26.449	87.001

Discussion Paper | Discussion Paper | Discussion Paper | Discussion Paper |

Table A3. Along stream water surface slope and grain size of bed materials.

Year	River	Thread	Slope	Discharge ($m^3 s^{-1}$)	Start Point Latitude (dd)	Start Point Longitude (dd)	End Point Latitude (dd)	End Point Longitude (dd)	Grain size (D50) (µm)
2013	Main Kosi	Braided	4.7×10^{-4}	175	26.490	86.935	26.363	86.786	224
2013	Main Kosi	Braided	4.6×10^{-4}	189	26.375	86.787	26.310	86.672	220
2013	Main Kosi	Braided	2.2×10^{-4}	960	26.057	86.469	25.886	86.433	170
2013	Main Kosi	Braided	1.9×10^{-4}	713	25.715	86.500	25.657	86.529	95
2013	Main Kosi	Single	4.8×10^{-5}	2251	25.419	87.170	25.410	87.249	–
2013	Seepage Channel	Single	4.2×10^{-4}	20	25.997	86.926	25.954	86.957	260

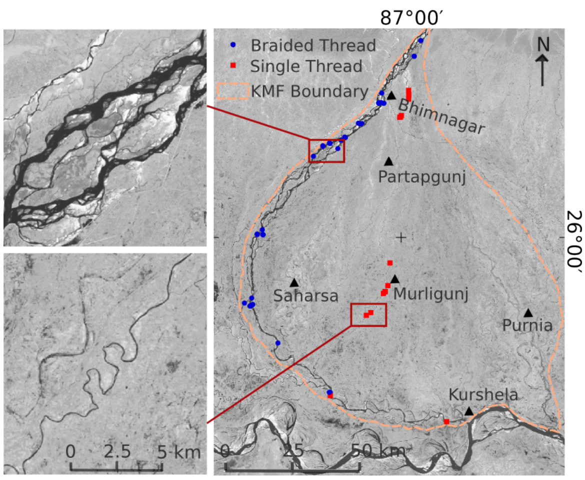

Figure 1. The Kosi megafan (KMF) boundary shown on LANDSAT-8 satellite image (acquired on, November 2013). Red and blue points on the image are showing the locations of the cross section measurements. Top and bottom left images are showing the typical pattern of braided and single thread rivers on the Kosi megafan surface (image source: US Geological Survey).

Discussion Paper | Discussion Paper | Discussion Paper | Discussion Paper |

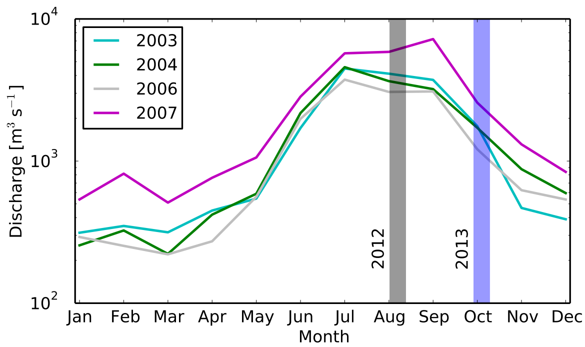

Figure 2. Four year trends of average monthly water discharge of the Kosi River (measured at the Kosi barrage, Bhimnagar). Gray and blue shades are showing the period of our measurements (source: discharge data obtained from investigation and research division Kosi project, Birpur).

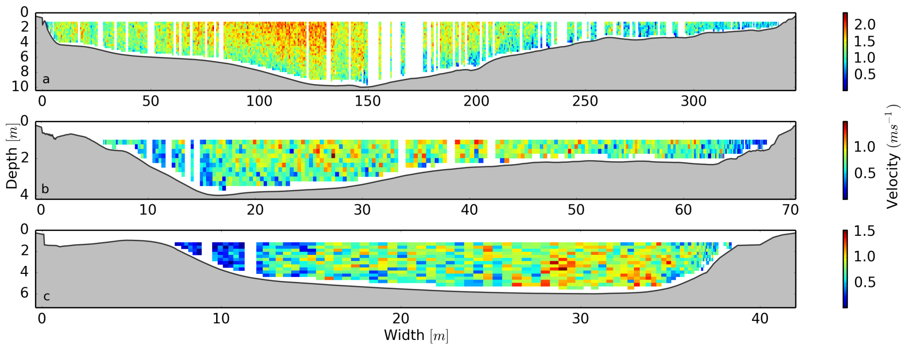

Figure 3. Velocity distribution across the single-thread channels of the Kosi fan. Measurement location of the section **(a)** 25.517, 86.737; **(b)** 25.857, 86.941 and **(c)** 25.776, 86.871.

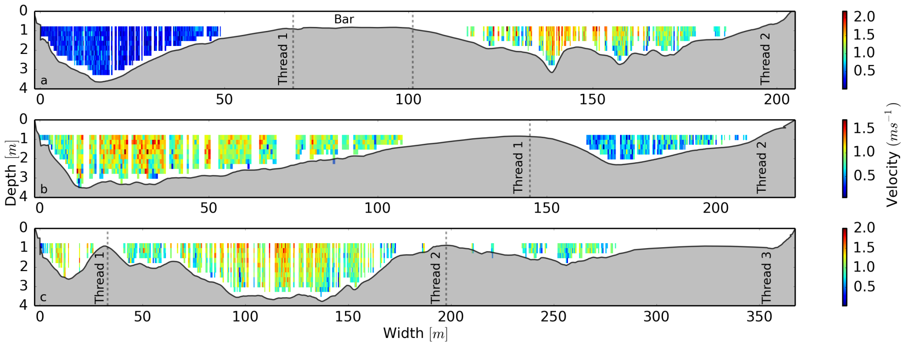

Figure 4. Velocity distribution across the braided threads of the Kosi fan. Measurement location of the section **(a)** 26.346, 86.707; **(b)** 25.807, 86.437 and **(c)** 25.807, 86.438. Dotted vertical lines in figure **(a)**, **(b)** and **(c)** are showing the criteria used to classify channel and bar portion within a cross-section.

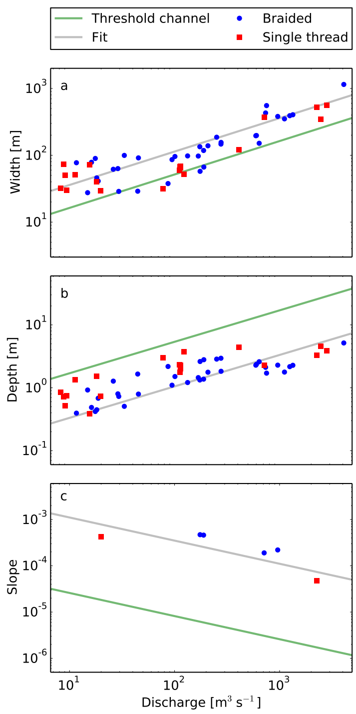

Figure 5. Threads width, depth and slope as functions of the water discharge. Solid green line is the threshold theory predicted curve. Solid grey line is fitted curve into the data points.

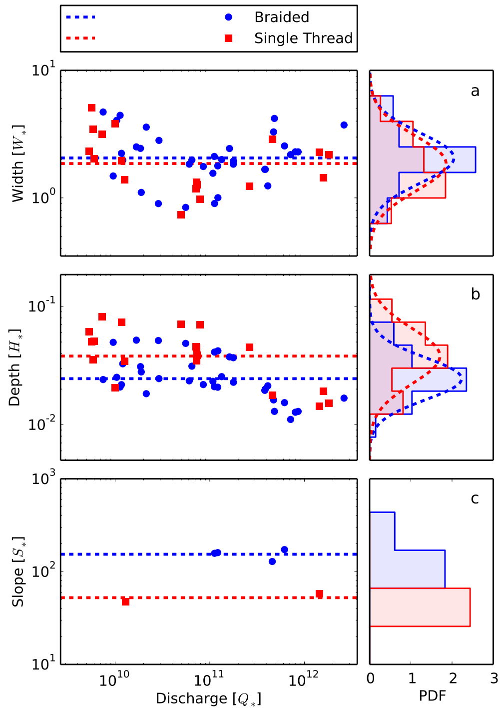

Figure 6. Dimensionless width (W_*), depth (H_*) and slope (S_*) of the Kosi threads as function of the dimensionless water discharge (Q_*). Dotted blue and red horizontal lines are the mean of the threads. Right side plots **(a)**, **(b)** and **(c)** are showing their corresponding probability density function (pdf).

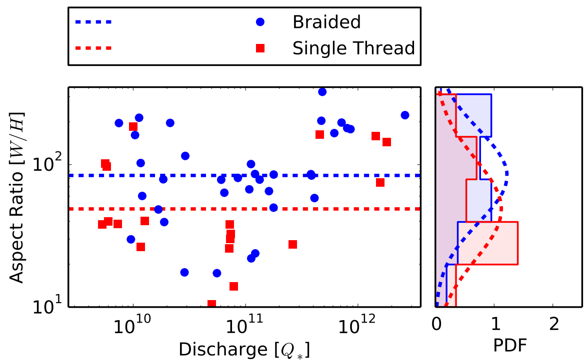

Figure 7. Threads aspect ratio (W/H) as function of the dimensionless water discharge (Q_*). Blue and red dotted horizontal lines are the mean of the threads. Right side plot is the probability density function of the threads and showing their distribution.